Krishna Mohan Singh
Sushanta Dutta
Sudhakar Subudhi
Nikhil Kumar Singh *Editors*

Fluid Mechanics and Fluid Power, Volume 7

Select Proceedings of FMFP 2022

Springer

Lecture Notes in Mechanical Engineering

Lecture Notes in Mechanical Engineering (LNME) publishes the latest developments in Mechanical Engineering—quickly, informally and with high quality. Original research reported in proceedings and post-proceedings represents the core of LNME. Volumes published in LNME embrace all aspects, subfields and new challenges of mechanical engineering.

To submit a proposal or request further information, please contact the Springer Editor of your location:

Europe, USA, Africa: Leontina Di Cecco at Leontina.dicecco@springer.com
China: Ella Zhang at ella.zhang@springer.com
India: Priya Vyas at priya.vyas@springer.com
Rest of Asia, Australia, New Zealand: Swati Meherishi at swati.meherishi@springer.com

Topics in the series include:

- Engineering Design
- Machinery and Machine Elements
- Mechanical Structures and Stress Analysis
- Automotive Engineering
- Engine Technology
- Aerospace Technology and Astronautics
- Nanotechnology and Microengineering
- Control, Robotics, Mechatronics
- MEMS
- Theoretical and Applied Mechanics
- Dynamical Systems, Control
- Fluid Mechanics
- Engineering Thermodynamics, Heat and Mass Transfer
- Manufacturing Engineering and Smart Manufacturing
- Precision Engineering, Instrumentation, Measurement
- Materials Engineering
- Tribology and Surface Technology

Indexed by SCOPUS, EI Compendex, and INSPEC.

All books published in the series are evaluated by Web of Science for the Conference Proceedings Citation Index (CPCI).

To submit a proposal for a monograph, please check our Springer Tracts in Mechanical Engineering at https://link.springer.com/bookseries/11693.

Krishna Mohan Singh · Sushanta Dutta ·
Sudhakar Subudhi · Nikhil Kumar Singh
Editors

Fluid Mechanics and Fluid Power, Volume 7

Select Proceedings of FMFP 2022

🐴 Springer

Editors
Krishna Mohan Singh
Department of Mechanical and Industrial
Engineering
Indian Institute of Technology Roorkee
Roorkee, Uttarakhand, India

Sushanta Dutta
Department of Mechanical and Industrial
Engineering
Indian Institute of Technology Roorkee
Roorkee, Uttarakhand, India

Sudhakar Subudhi
Department of Mechanical and Industrial
Engineering
Indian Institute of Technology Roorkee
Roorkee, India

Nikhil Kumar Singh
Department of Mechanical and Industrial
Engineering
Indian Institute of Technology Roorkee
Roorkee, Uttarakhand, India

Contents

Measurement Techniques in Fluid Mechanics

About the Editors

Prof. Krishna Mohan Singh is Professor in the Department of Mechanical and Industrial Engineering at Indian Institute of Technology (IIT) Roorkee. His research interests include the areas of computational mechanics, development of novel parallel algorithms, meshfree methods, shape and topology optimization, fluid dynamics, DNS/LES of turbulent flows, CAE, computer-aided analysis and design of thermo-fluid and multi-physics systems, computational fluid dynamics, modeling and simulation of flow and heat transfer in turbomachines, transport and energy systems.

Prof. Sushanta Dutta is Professor in the Department of Mechanical and Industrial Engineering at Indian Institute of Technology (IIT) Roorkee. His research interests are in the areas of experimental fluid mechanics, experimental heat transfer, optical measurement techniques, active and passive control of flow field, wake dynamics, turbulence study, Schlieren, HWA, PIV, LCT, PSP, microfluidics and heat transfer augmentation using phase change material.

Prof. Sudhakar Subudhi is Professor in the Department of Mechanical and Industrial Engineering at Indian Institute of Technology (IIT) Roorkee. His research interests are in the area of experimental heat transfer and fluid mechanics, heat transfer enhancement of natural and forced convection in water/nanofluids, natural ventilation and unconventional energy systems.

Dr. Nikhil Kumar Singh is Assistant Professor in the Department of Mechanical and Industrial Engineering at Indian Institute of Technology (IIT) Roorkee. His broad research interests include direct numerical simulations of two-phase flows and phase change, computational fluid dynamics and heat transfer, numerical methods and turbulent flows.

Renewable Energy

Performance Exploration of Impinging Jet Solar Air Heater: A Comparative Study

Amitesh Sharma, Sushant Thakur, Prashant Dhiman, and Rakesh Kumar

Abstract Given the imminent depletion of fossil fuels, the present scenario relies on capturing solar energy. The current study compares experimental trials of traditional SAH with alternative impinging jet ribbed solar air heater designs. The experimental investigation is investigated by increasing the Re from 4000 to 16,500 and comparing the results. The geometric parameters and jet parameters used in the investigation were $e/d_{hd} = 0.043$, $P/e = 10$, $\alpha = 55°$, $X_{st}/d_{hd} = 0.40$, $Y_{sp}/d_{hd} = 0.84$, and $d_j/d_{hd} = 0.064$. The impinging jet with multi-V-shaped ribs outperformed the V-shaped ribbed SAH, with a reported thermohydraulic efficiency of 3.301 compared to 2.05 for the V-shaped ribbed SAH and 1.83 for the impinging jet flat-plate solar air. It establishes that when active and passive heat transfer approaches are coupled, heat transfer enhancement and THEP are increased. The findings were also compared to traditional SAH.

Nomenclature

SAH	Solar air heater
A_o	Duct opening area, m^2
C_p	Specific heat at const. pressure, J kg^{-1} K^{-1}
d_{hd}	Hydraulic dia. of the channel, m
A_p	Absorber plate area, m^2
C_d	Coefficient of discharge of orifice plate

A. Sharma (✉) · S. Thakur · P. Dhiman
Mechanical Engineering Department, N.I.T, Hamirpur, India
e-mail: amitesh.jngec@gmail.com

A. Sharma · R. Kumar
Mechanical Engineering Department, M.G. Government Engineering College, Jeori Shimla, H.P, India

H	Vertical channel height, m
e	Wire roughness height, m
m	Flow rate of air, kg s^{-1}
L	Length of testing section, m
P	Roughness pitch, m
k_a	Air thermal conductivity, W m^{-1} K
h	Convective coefficient, W m^{-2} K
Q_f	Heat exchange rate, W
ΔP_d	Pressure decrement crosswise in the testing section, N m^{-2}
ΔP_o	Pressure decrement in orifice meter, N m^{-2}
T_{in}	Entry air temp. in the conduit, K
T_{out}	Exit air temp. in plenum, K
T_{mp}	Average plate temperature, K
T_{mf}	Mean temp. of air, K
V	Fluid speed, m s^{-1}
W	Conduit breadth, m Dimensionless factors/numbers
e/d_{hd}	Relative wire rib roughness height
f_s	Friction factor of conventional SAH
Nu	Nusselt number
Nu$_{\text{s}}$	Nusselt number of conventional SAH
P/e	Relative roughness pitch
w/W	Width ratio
Pr	Prandtl number
Re	Reynolds number
f_p	Friction penalty of a roughened surface
$X_{\text{st}}/d_{\text{hd}}$	Streamwise impinging jet pitch ratio
$Y_{\text{st}}/d_{\text{hd}}$	Spanwise impinging jet pitch ratio
THEP	Thermohydrodynamic efficiency parameter

Symbols: (Greek)

α	Attack angle
β	Fraction of hole distance corresponding of pipe width
ρ_{air}	The density of fluid, kg m^{-3}
ρ_{air}	Density of flowing air at mean temperature, kg m^{-3}
ϑ	Kinematic viscosity, m^2 s^{-1}

1   Introduction

Solar insolation is a pure, plentiful, and limitless source of power. Research on renewable energy is sorely needed in light of the present fossil fuel dilemma [1]. A solar air heater (SAH) is a tool for obtaining solar heat energy to be used in commercial and agricultural purposes [2]. Heating systems and air conditioning (SAH) are preferred over solar water heaters (SWH) due to their usage in a number of technical applications, such as the drying of paper and pulp, whereas SWH's uses are quite constrained. Second, the simple design, lack of scaling-fouling, corrosion, leakage problems, and safety features of SAHs make them safe to use [3]. Despite its numerous advantages, it has one disadvantage: poor performance due to air's low heat transfer coefficient [4].

Numerous techniques have been created to increase SAH efficiency and encourage heat exchange between the absorbing surface and air [5]. The techniques are categorized as active techniques, passive techniques, and combination of both active and passive techniques [6]. The absorber plate is suitable modified by arrangement of ribs underneath the absorber plate which results in distortion of laminar sublayer resulting in heat transfer augmentation [7]. Design modifications are done by the arrangement of extended surfaces [8, 9] incorporating baffles suitably on absorber plate [10] and utilizing the impingement of flowing fluid on the absorber plate for boosting the turbulence [11]. The jet impingement approach is a good way to improve heat transfer between air and a hot surface [12]. Several researchers investigated this process and reported on it in experimental and numerical investigations. Based on jet impingement physics, Chaudhary and Garg developed a mathematical model for solar air heaters, with findings indicating a 26% improvement in efficiency and a maximum temperature rise of 15.5 °C at airflow rates ranging from 50 to 250 kg/hm^2 with a 10 cm conduit depth and 2.0 m duct length [13]. Chauhan and Thakur conducted an experimental procedure of modified impinging jet SAH, with reported maximum efficiency of 70% recorded by adjusting jet hole diameter, streamwise jet pitch, and spanwise jet pitch [14]. The effectiveness of an unglazed SAH with an impinging jet was investigated by Belusko et al., and it was shown that jet-to-jet distance is paramount factor in increasing thermal efficiency [15]. Singh et al. evaluated impinging jet behavior in a dual-passage rectangular duct with a modified corrugated wavy impinging jet plate. The highest thermal performance improvement of roughly 94% was achieved with 0.48% perforation of the impinging jet plate and 98% bed porosity [16]. Maithani et al. used jet impingement on an absorber plate having hemispherical protrusions slightly below the jet holes in order to provide impingement over the protrusions and produce turbulence. The maximum thermal hydraulic efficiency measurement was 3.01 [17]. Kannan et al. conducted investigation under outdoor circumstances, a suitably adapted SAH with a pin–fin absorber plate, and compared this with a normal SAH, and the output air temperature was increased from 2° to 7 °C with improved energy, thermohydraulic, and exergy efficiency [18].

According to the prior research, the impinging jet method is extensively employed for enhancing heat transfer in a variety of applications. Only few works have

been conducted to investigate the interaction of cylindrical wire-shaped ribs with impinging air jet SAH. The current study fills this void by examining the thermal behavior of cylindrical wired ribs positioned underneath the absorber plate and applying a variety of geometric parameters for rib roughness in cylindrical wire-shaped ribs. The current experimental investigation is a comparison of the increased thermal behavior of an impinging jet on a flat-plate solar air heater and an impinging air ribbed solar air heater with ribs installed on a V-shaped pattern and a multi-V-shaped pattern with a conventional SAH.

2   Experimental Setup

An indoor test facility for assessing roughened absorber plate has been established in line with the ASHRAE standard [19]. A test facility has been built based on this idea, as illustrated in Fig. 1. It was an open-loop system with a rectangular route comprising components for entry, testing, and exit.

The test component of the rectangular channel has a cross-section of 300×25 mm and a length of 1400 mm. The entry and exit parts are respectively 600 and 400 mm in dimension, equivalent of $5\sqrt{W_d H_d}$ & $2.5 \sqrt{W_d H_d}$ as per ASHRAE protocols. As a result, the flow may be presumed to be completely developed across the length of the test portion. A variac is used to govern a steady heat flow of approximately 1000 W/m^2. The mass flow through the conduit is measured using a U-tube. A digital micro-manometer of TSI made with a least count of 0.1 Pa was used to monitor the pressure change over the jet impingement test segment. The average temperature of
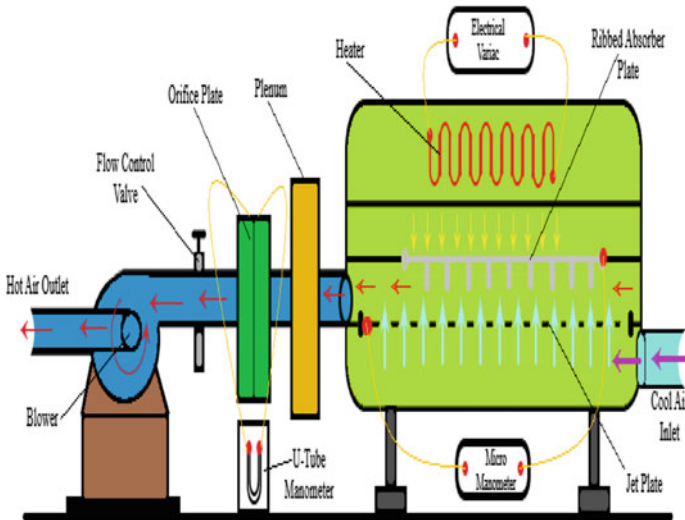
Fig. 1 Test rig

Table 1 Lists the parameters that were chosen for the experiment

S no.	Parameters of investigation	Range
1	Re	4000–16,500
2	Width ratio (w/W)	01 and 05
3	Relative roughness ht. (e/d_{hd})	0.043
4	Relative roughness pitch (P/e)	10
5	Attack angle (α)	55^0
6	Streamwise jet hole pitch ratio (X_{st}/d_{hd}),	0.40
7	Spanwise jet hole pitch ratio (Y_{sp}/d_{hd})	0.84
8	Jet hole diameter ratio (d_j/d_{hd})	0.064

air at the intake and exit portions, as well as the temperature of the absorbing surface, was measured at 18 places using calibrated J-type thermocouples with an accuracy of 0.1 °C. The air was blown through the rectangular conduit using a 3-HP centrifugal blower. The experiment was started by setting the appropriate set of geometric and flow parameters on the jet plate arrangement, and the operational conditions were assured by utilizing a gate valve to govern the mass flow rate of air.

The various parameters selected for the study are presented in Table 1.

3 Confirmation of the Experimental Procedure

The created setup facility was approved for a conventional SAH without any obstructions in the passage of the flow regimes, as required by the laws. The estimated results from an experimental run were equal to the projected values of the Nu and friction penalty determined using an empirical relationship well acknowledged by various researches for assessing classic SAH. The Dittus-Boelter correlation and Gnielinski equation as given in Eqs. (1, 2) for Nusselt number, the modified Blasius equation as represented in Eq. (3), and Petukhov equation as represented in Eq. (4) were used to obtain the projected values for conventional SAH in validating friction factor [7]. As shown in Fig. 2, the mean absolute deviation in this conformity for Nusselt number estimated using Gnielinski and Dittus-Boelter correlations was 5.06% and 6.8%, respectively. The mean absolute deviation of friction penalty from modified Blasius and Petukhov empirical correlations and experimental values were 3.5 and 6.1% as represented in Fig. 3**.** The lower percentage of mean absolute deviation proves the setup acceptability and validation of the experimental facility and its use in future test concerning planned study, leading to logical acceptance of the test rig.

$$Nu_s = 0.023\text{Re}^{0.8}\text{Pr}^{0.4} \tag{1}$$
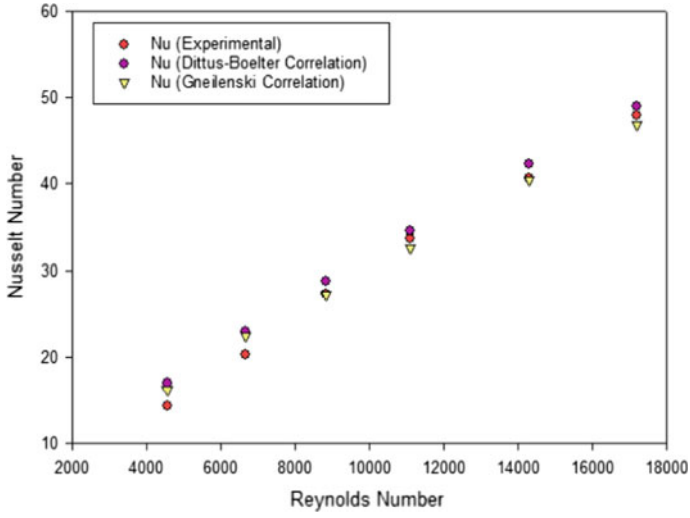
Fig. 2 Validation for Nu
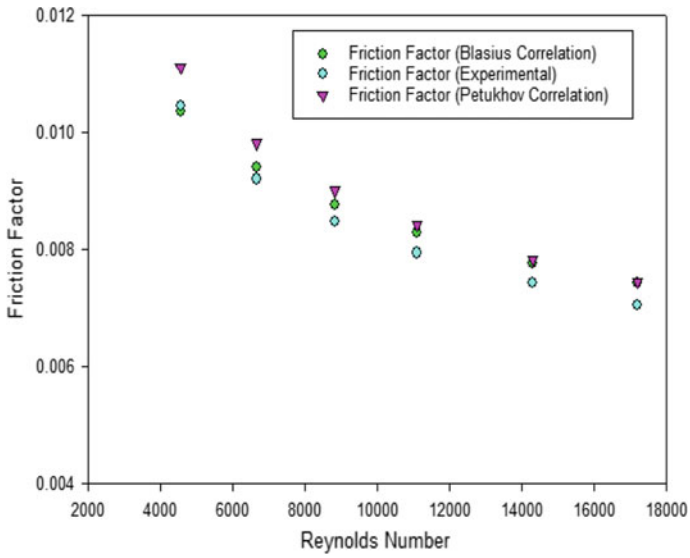
Fig. 3 Validation for friction factor

$$Nu_s = \frac{(f/2)(\mathrm{Re} - 1000)\,\mathrm{Pr}}{1 + 12.7\big([f/2]^{0.5}3\big)(\mathrm{Pr}^2 - 1)} \tag{2}$$

$$f_s = 0.085\,\mathrm{Re}^{-0.25} \tag{3}$$

$$f_s = (1.58 \ln \text{Re} - 3.82)^{-2} \tag{4}$$

3.1 Formula Used

1. Heat gain by fluid:

$$Q_f = \dot{m}C_p(T_{out} - T_{in})$$

2. Mass flow rate of working fluid:

$$\dot{m} = C_d A_o \left[\frac{2\rho_{\text{air},0}\Delta P_o}{1 - \beta^4} \right]^{1/2}$$

3. Friction factor:

$$f = \frac{2(\Delta P)_d D_h}{4\rho_{air} L V^2}$$

4. Convective heat transfer coefficient:

$$h = \frac{Q_a}{A_p(T_{mp} - T_{mf})}$$

5. $Nu := \frac{hD_h}{k_{air}}$.

3.2 THEP

A lot of studies have looked into the usage of turbulence promoters to improve the thermal behavior of SAH. This advantage, however, comes at the expense of a pressure loss, which needs a large pumping effort to move the air through the pipe. As a result, in order to establish the setup for effective performance, the heat transfer and friction characteristics must be examined concurrently, a process known as "thermohydraulic performance," [20] as mentioned in Eq. (5)

$$\eta_{\text{THEP}} = \left[(Nu_{\text{roughened}}/Nu_{\text{smooth}})/(f_{\text{roughened}}/f_{\text{smooth}})^{\frac{1}{3}} \right] \tag{5}$$

4   Result and Discussion

This experimental comparative study determines the Nu symbolizing heat transfer increase, friction coefficient, and THEP for a given range of variables used in a redesigned impinging jet solar air heater.

4.1   Heat Gain

The augmentation in Nusselt number represents the heat gain. Figure 4 demonstrates the relationship between Nu and Re within a set of parameters. The fixed geometric and jet parameters were $w/W = 1$ and 5 (width ratio), $P/e = 10$ (relative roughness pitch), $e/d_{\text{hd}} = 0.043$ (relative rib roughness height), $\alpha = 55°$ (attack angle), $X_{st}/d_{\text{hd}} = 0.40$ (streamwise pitch), $Y_{st}/d_{\text{hd}} = 0.84$ (spanwise pitch), and jet hole diameter $(d_j/d_{\text{hd}}) = 0.064$. In typical solar air heaters, heat transmission to the air is limited by a viscous layer formed near the absorber plate, and the impinging jet causes turbulence and promotes heat transfer augmentation, stated to as the passive heat transfer enhancement strategy. As shown in the illustration Fig. 5, a modified absorber plate is used, with V-patterned ribs positioned beneath the absorber plate and a jet impinging from the bottom via the jet plate. This is an amalgamation of active and passive manners of heat transfer, and the results show that as Re increases, Nu increases for both impinging jet and impinging jet V patterned ribs, and the results are also compared to conventional solar air heaters, as shown in Fig. 4, with the maximum Nu reported for multi-V-patterned impinging jet SAH and secondly by V-patterned impinging jet SAH.

As a result, the arrangement in which the ribs were fastened throughout the whole length of the absorber plate was optimal for heat exchange. To push fluid from the cooler zone (internal core) toward the multi-V obstacle wall, the impingement jets have two separate rotating vortices. As a result, the lower impingement jets become entrained in the primary flow. Boundary layer development was halted due to heat transmission among the multi-V ribs, which was triggered by the mixing of inner stream with the main stream. With an increase in Re, the convective resistance in the boundary layer decreased, resulting in a thinner boundary layer and a greater Nu. As a result, there was significant turbulence where the impinging jets separated and merged with the main stream. This was located behind the ribs. There was a rise in HT from the absorber plate to the air as the number of vortices rose as in multi-V ribs in comparison with other designs.
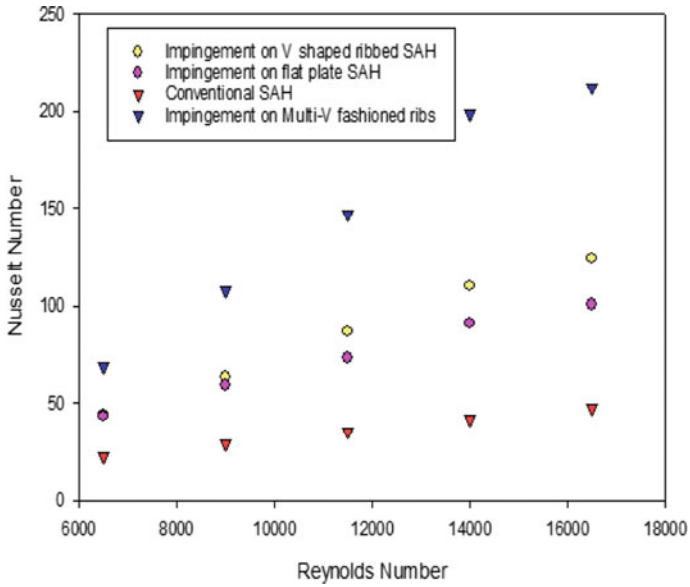
Fig. 4 Variation of Nusselt number with Re
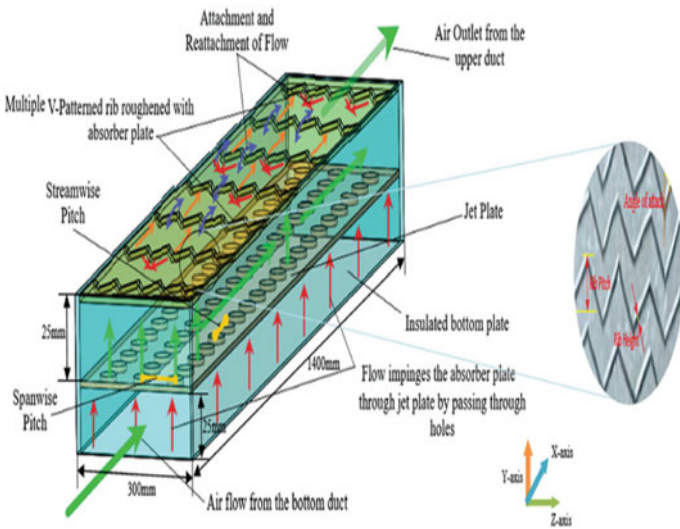
Fig. 5 Schematic diagram and flow pattern [5]
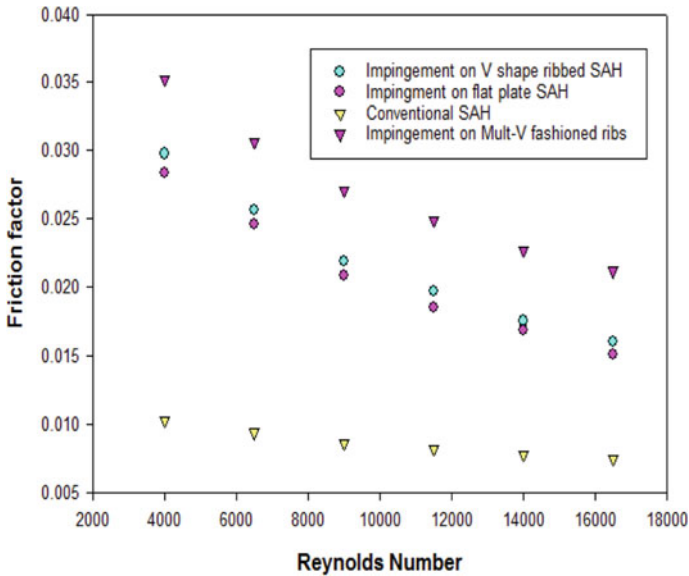
Fig. 6 Variation of Friction factor with Re

4.2 Frictional Characteristics

Figure 6 shows the relationship between f and Re for a set of selected parameters. With rising Re, the value of f continues to decrease. As Re increases, so does air penetration into the ribs, resulting in a continual reduction in pressure drop. Furthermore, the jet spacing is carefully selected to reduce jet interference. When the width-to-expansion value ratio was adjusted from 1 to 5, a corresponding rise in the number of secondary stream jets was observed. In this way, a sequence of V-shaped ribs on the absorber plates can increase the friction factor to a maximum value within the range of the design's specifications. The frictional cost introduced by the partitioning of the flow may be used to investigate the vortex structures. Nu rises when pressure builds up in the vortex. An increase in Nu, as is the case with most targets, occurs when the flow increases its pumping force around the SAH, as seen above. The frictional factor recorded for V-patterned ribbed impinging jet SAH is 0.0297. The highest value recorded for multi-V-patterned ribs signifies that augment in heat transfer leads to enhancement in pressure drop.

4.3 THEP

Thermohydraulic performance is dimensionless parameter that denotes performance of modified SAH. Figure 7 illustrates THEP variation with Re for fixed geometric
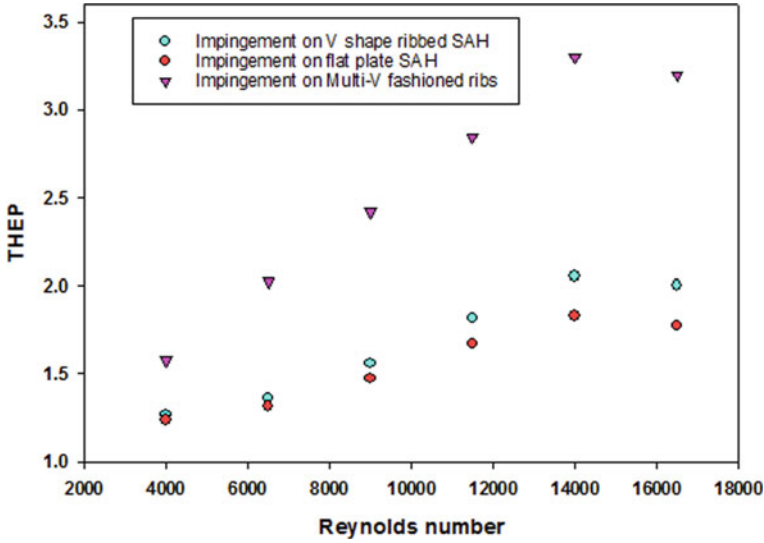
Fig. 7 Thermohydraulic efficiency parameter variation with Re

and jet parameters. The maximum THEP reported is for Reynolds number 14,500 for all designs, i.e., impinging jet SAH, impinging jet ribbed SAH (V and multi-V ribs) with maximum reported value of 3.301 for impinging jet multi-V-patterned ribs. The rise and fall that were seen in the findings of thermohydraulic efficiency may be attributed to an increase in the pumping power above the thermal gain at a certain value of mass flow rate in relation to the geometrical parameters, and this value offers the optimum value.

5   Conclusions

The present study is performed to conclude the comparison of impinging air and impinging air ribbed SAH, in which ribs are organized in V pattern. The fixed value of various parameter is $w/W = 1$ and 5, $P/e = 10$, $e/d_{hd} = 0.043$, $\alpha = 55°$, $X_{st}/d_{hd} = 0.40$ (streamwise pitch), $Y_{st}/d_{hd} = 0.84$, and jet hole diameter (d_j/d_{hd}) = 0.064. The results clearly showed that when jet impingement is combined with roughness, heat transfer augmentation increases with a certain rise in friction factor. The results clearly showed that when jet impingement is combined with roughness, heat transfer augmentation increases with a certain rise in friction factor. The study's findings may be summarized as follows:

- The highest THEP is reported as 3.301 for impinging jet multi-V-patterned ribbed modified SAH.

- When equated to usual conventional SAH, there is a 4.70 times enhancement in Nu and a 2.92 times augmentation in friction factor in this research in the option of impinging jet multi-V-patterned ribbed modified SAH with width ratio of 5.

References

1. Phu NM, Tuyen V, Ngo TT (2019) Augmented heat transfer and friction investigations in solar air heater artificially roughened with metal shavings. J Mech Sci Technol 33(7):3521–3529. https://doi.org/10.1007/s12206-019-0646-x
2. Singh I, Singh S, Vardhan S (2021) Heat transfer and fluid flow characteristics of solar air heater duct with non-uniform ribs. J Mech Sci Technol 35(1):343–350. https://doi.org/10.1007/s12206-020-1234-9
3. Sharma S, Das RK, Kulkarni K (2021) Computational and experimental assessment of solar air heater roughened with six different baffles. Case Stud Therm Eng 27:101350. https://doi.org/10.1016/j.csite.2021.101350
4. Kumar R, Goel V, Bhattacharyya S, Tyagi VV, Abusorrah AM (2022) Experimental investigation for heat and flow characteristics of solar air heater having symmetrical gaps in multiple-arc rib pattern as roughness elements. Exp Heat Transf 35(4):466–483. https://doi.org/10.1080/08916152.2021.1905752
5. Sharma A, Thakur S, Dhiman P (2022) Jet impingement in a V-rib roughened solar air heater: an experimental approach. Energy Sourc Part A Recover Util Environ Eff 44(3):6970–6984. https://doi.org/10.1080/15567036.2022.2105988
6. Mousavi Ajarostaghi SS, Zaboli M, Javadi H, Badenes B, Urchueguia JF (2022) A review of recent passive heat transfer enhancement methods. Energies 15(3):986. https://doi.org/10.3390/en15030986
7. Yadav SK (2021) Thermal performance evaluation of arc rib having symmetrical wide gaps and staggered elements and additional narrow gap in each arc segment used in absorber surface of solar air heater. Appl Sol Energy 57(3):192–197. https://doi.org/10.3103/S0003701X21030105
8. Josyula T, Singh S, Dhiman P (2018) Numerical investigation of a solar air heater comprising longitudinally finned absorber plate and thermal energy storage system. J Renew Sustain Energy 10(5):055901. https://doi.org/10.1063/1.5035136
9. Goel AK, Singh SN (2019) Performance studies of a jet plate solar air heater with longitudinal fins. Int J Ambient Energy 40(2):119–127. https://doi.org/10.1080/01430750.2017.1372808
10. Chamoli S, Thakur NS (2015) Effect of roughness height ratio in V down perforated baffle roughness on thermohydraulic performance of solar air heater: an experimental study. Int J Ambient Energy 36(5):242–247. https://doi.org/10.1080/01430750.2013.853206
11. Kumar R, Nadda R, Rana A, Chauhan R, Chandel SS (2020) Performance investigation of a solar thermal collector provided with air jets impingement on multi V-shaped protrusion ribs absorber plate. Heat Mass Transf 56(3):913–930. https://doi.org/10.1007/s00231-019-02755-2
12. Shukla AK, Dewan A (2017) Flow and thermal characteristics of jet impingement: comprehensive review. Int J Heat Technol 35(1):153–166. https://doi.org/10.18280/ijht.350121
13. Choudhury C, Garg HP (1991) Evaluation of a jet plate solar air heater. Sol Energy 46(4):199–209. https://doi.org/10.1016/0038-092X(91)90064-4
14. Chauhan R, Thakur NS (2014) Investigation of the thermohydraulic performance of impinging jet solar air heater. Energy 68:255–261. https://doi.org/10.1016/J.ENERGY.2014.02.059
15. Belusko M, Saman W, Bruno F (2008) Performance of jet impingement in unglazed air collectors. Sol Energy 82(5):389–398. https://doi.org/10.1016/J.SOLENER.2007.10.005
16. Singh S, Chaurasiya SK, Negi BS, Chander S, Nemś M, Negi S (2020) Utilizing circular jet impingement to enhance thermal performance of solar air heater. Renew Energy 154:1327–1345. https://doi.org/10.1016/j.renene.2020.03.095

17. Maithani R, Kumar A, Raghav G, Nagpal M, Kumar B (2021) Thermal analysis of jet impingement on hemispherical protrusion on heated surface. Exp Heat Transf 34(7):662–677. https://doi.org/10.1080/08916152.2020.1808117
18. Kannan C, Mohanraj M, Sathyabalan P (2021) Experimental investigations on jet impingement solar air collectors using pin-fin absorber. Proc Inst Mech Eng Part E J Process Mech Eng 235(1):134–146. https://doi.org/10.1177/0954408920935301
19. ASHRAE (1977) Method of testing to determine the thermal performance of solar collectors. (ASHRAE standard 93–7)
20. Webb RL, Eckert ERG, Goldstein RJ (1972) Generalized heat transfer and friction correlations for tubes with repeated-rib roughness. Int J Heat Mass Transf 15(1):180–184. https://doi.org/10.1016/0017-9310(72)90179-2

Performance Evaluation of Single Pass Solar Air Heater with Stepped-Type Arrangement of Metal Foam by a Numerical Study

Rawal Diganjit and N. Gnanasekaran

Abstract A solar air heater is easy to build and easy to use for drying applications, room heating purposes, etc. In the present study, single-pass forced convection rectangular-type solar air heater is studied numerically. The copper metal foam with 0.92 porosity is used for case (a) empty channel, cases (b) to (e) comprising of different stepped-type arrangements, and case (f) fully filled metal foam condition and studied numerically to obtain outlet temperature, pressure drop and the performance factor of the solar air heater. The Reynolds number is varied from 4401 to 5868. Based on this range of Reynolds number RNG k-ε model with enhanced wall function is adopted for numerical simulations. The local thermal equilibrium model is used to simulate the porous zone. The Rosseland radiation model has been chosen with solar ray tracing method. The case (c) is the best stepped-type arrangement to get same outlet temperature compared to fully filled metal foam case (f). Hence, the material cost is minimized. The temperature rise is 8.89% more compared to empty channel solar air heater. Case (c) has less pressure drop compared to other metal foam arrangements. The performance factor for case (c) is 2.03.

Keywords Single pass · Solar air heater (SAH) · Metal foam · Performance factor · Forced convection

Nomenclature

R_e	Reynolds number [-]
ε	Porosity [%]
T_s	Solid temperature [K]
T_f	Fluid temperature [K]
T_{out}	Outlet temperature [K]

R. Diganjit · N. Gnanasekaran (✉)

Department of Mechanical Engineering, National Institute of Technology, Mangalore, Karnataka 575025, India

e-mail: Gnanasekaran@nitk.edu.in

ΔP Pressure drop [Pa]
CFD   Computational fluid dynamics [-]
SAH   Solar air heater [-]
ρ Density [kg/m^3]
Cp Specific heat capacity [kJ/kg K]
k Thermal conductivity [W/m K]
μ Kinematic viscosity [Ns/m^2]

1   Introduction

Solar energy is easily available on earth. It has zero cost; so, there is a scope to utilize this solar energy for human comfort. The solar air heater has four main parts, i.e., absorber plate, transparent cover, insulation, and outer frame of the solar air heater. The absorber plate absorbs the solar radiation and heats the incoming air. The air passes through the space between the glass and absorber plate. The metal foam is used due to its low density, high superficial area-to-volume ratio, and high strength. The metal foam is used to maximize the heat transfer rate in solar air heater [1], heat exchangers [2], electronic cooling devices, etc.

2   Literature Review and Objectives

Saedodin et al. [1] performed numerical and experimental analyses using single-pass flow. They used porous metal foam having bed dimensions of 70×12 mm. The control volume method and local thermal equilibrium (LTE) model have been adopted through test channel to get thermal performance, and pressure drop. The numerical and experimental analyses of porous medium results give increased thermal efficiency and Nusselt number up to 18.5% and 82% respectively. Kansara et al. [3] investigated the performance of flat-plate collector using internal fins and porous media by using solar simulator. The rise in temperature of air with fins and porous media is 8.19% and 16.17%, respectively, than an empty channel. Maximum rise is 115.9 K for copper foam, and minimum is 110.4 K for steel foam. Anirudh et al. [4] studied performance improvement of a flat-plate solar collector with intermittent porous blocks by using numerical analysis of FPSC. The porous resistances are higher in amplitudes for low permeability. The values vary for Darcy–Brinkman compared to Extended Darcy–Brinkman–Forchheimer model. Singh et al. [5] performed experimental and numerical investigations of a single and double pass using porous serpentine wavy wire mesh in solar air heater. Best thermal and thermohydraulic efficiencies for 93% porous double-pass serpentine-packed bed solar air heater are achieved. The thermohydraulic performance for serpentine presents 24.33% than flat-packed bed solar air heater. Huang [6] reported a numerical study of enhanced forced convection

in a channel of solar water collector using multiple metal foam blocks. With the help of Darcy–Brinkman–Forchheimer flow model and local thermal non-equilibrium model, the study includes thermo-flow fields inside the porous media. Valizade et al. [7] studied experimentally the thermal behavior of direct absorption parabolic collector using copper metal foam. The maximum thermal efficiency for full metal foam and semi-metal foam are 171.2% and 119.6%, respectively, than free-channel metal foam. Wang et al. [8] worked on experimental study of latent thermal energy storage system with copper metal foam for further solar applications. Silicon oil was utilized as heat transfer fluid. Hence, temperature uniformity improved and the reduction in time for melting the mixture by 37.6%. Xiao et al. [9] investigated thermal performance analysis of a solar energy storage using copper foam/nanosalt. The results show that the time duration of heat storage process at heating temperature of 160° is reduced by 58.5%. Jouybari et al. [10] experimentally investigated the use of metal foam using nanofluid to improve thermal performance. The performance evaluation criterion is used to reduce the pressure drop and increase the heat transfer. With the help of metal foam and nanofluid, the performance evaluation criteria increased more than 1% at a lower flow rate. The increase in nanofluid concentration increases the performance evaluation criteria. Rajarajeswari et al. [11] reported numerical and experimental results in porous and non-porous solar air heaters. Two types of screen wire mesh WSM-I and WSM-II having different porosities and characteristics are used. The increase in thermal efficiency for WSM-I and WSM-II is 5–17% and 5–20% respectively with mass flow rate from 0.01 to 0.05 kg/s. Jadhav et al. [12] accomplished the numerical study of horizontal pipe in the presence of metal foam. Darcy-extended Forchheimer (DEF) and local thermal non-equilibrium (LTNE) models were used. The novelty of the work is the selection of suitable flow and thermal models to find the heat transfer in metallic foams.

From the above literature, it is understood that metal foam is the best option to increase heat transfer rate. At the same time, the pressure drop increases due to the resistance offered by the metal foams. To overcome this issue, researchers have attempted several methods, but stepped-type arrangement is not studied till date in the literature. This type of arrangement not only increases the heat transfer but also decreases the pressure drop. Hence in this paper, four different stepped arrangements are considered. The objective of this work is to study the different stepped-type arrangement of metal foam to increase outlet temperature and reduce pressure drop.

3   Materials and Methods

A rectangular channel-type SAH experimental study of Rajarajeswari [11] is considered as a reference work for this numerical analysis of heat transfer through porous media like metal foam. The width is modified in this analysis. Width is considered to be 1 m because the industrial solar air heater absorber plate area is in general 2 m². The schematic diagram and numerical geometry are shown in Fig. 1.
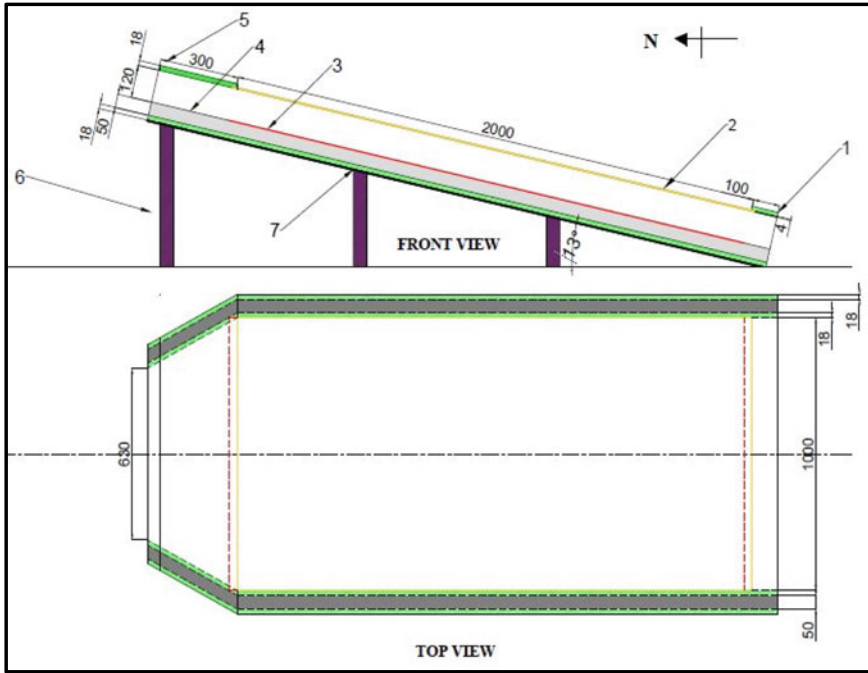
Fig. 1 Detailed schematic layout of SAH, 1 wooden material for entrance section, 2 toughened glass, 3 aluminum absorber plate, 4 insulation, 5 wooden material for exit section, 6 M S steel stand for support, and 7 wooden materials for the frame as an outer box of the solar air heater

It consists of $2 \times 1 \times 0.12$ (m) as a length, width, and height of solar air heater, respectively. The top plate is transparent toughened glass with 0.004 m thickness. The bottom absorber plate is considered as aluminum with 0.0005 m thickness. The wood material is considered as an insulation material to reduce heat losses from side wall and bottom wall of SAH. The location for the present study is the Department of Mechanical engineering, National Institute of Technology, Karnataka, India. The longitude and latitude for the location are 74.7951 ° and 12.9958 °, respectively. So, the SAH is tilted at 13 ° to facing south. The absorptivity of black painted aluminum plate is taken as 0.95 and wall is opaque. The transparent cover has 0.1 absorptivity and 0.9 transmissivity (Fig. 2).

3.1 Computational Details and Boundary Conditions

The 3D geometry is drawn with the help of Ansys Fluent 2019 R3 software. The solar air heater is divided into three parts, i.e., entrance zone, test zone, and exit zone. The fluid as air is taken for this analysis. The mesh for this domain is linear mesh.
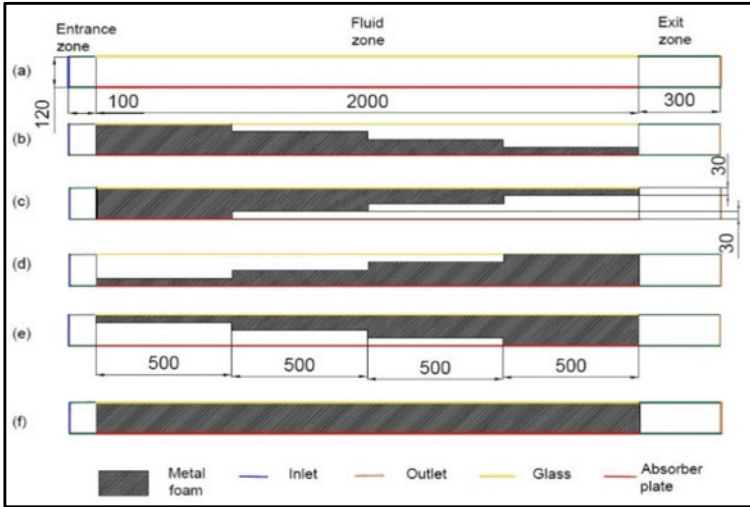
Fig. 2 Schematic diagram of stepped metal foam arrangement in solar air heater case **a** empty channel, case **b**, case **c**, case **d**, case **e**, and case **f** fully filled metal foam

The maximum skewness of the meshing is 0.3526. For the setup, pressure-based solver is taken with absolute velocity. The steady flow is considered for the present analysis. The RNG k-ε model with enhanced wall function is employed for the turbulent flow of air. The Reynolds number for the present study is from 4401 to 5868. The Rosseland radiation model is used with solar ray tracing method for complete analysis as mentioned in [11]. The sunshine factor is taken as 1. For direct beam radiation and diffuse radiation, the solar calculator is selected to get accuracy. All the simulations are done for the date 15 April. The maximum solar intensity for the day is 13:00 pm. Hence, 13:00 pm is considered for further analysis. The material properties are taken as mentioned in Table 1.

In the cell zone conditions, the porous zone is included to increase the heat transfer rate, i.e., to increase the outlet temperature of solar air heater by using metal foam. The porosity and pore diameter of metal foam are mentioned in [13]. The same configurations are used for comparing the heat transfer rate of solar air heater in the present study. The details are given in Table 2.

Table 1 Material properties used for CFD simulations

	Air	Aluminum	Glass	Wood
Density (ρ) kg/m^3	1.225	2719	2500	700
Specific heat capacity (Cp) kJ/kg K	1006.43	871	670	2310
Thermal conductivity (k) W/m K	0.0242	202.4	0.7443	0.173
Kinematic viscosity (μ) Ns/m^2	1.789 E-05	–	–	–

Table 2 Details of copper metal foam

	Copper metal foam [13]
Pore diameter (mm)	0.216
Pitch (mm)	2.324
Porosity	0.92
Viscous resistance	6,082,725.061
Inertial resistance	148.97

Table 3 Boundary condition considered for CFD analysis

	Conditions
Inlet velocity	0.3, 0.35, and 0.4 m/s and its turbulent intensity 5.6063%, 5.4993%, and 5.4083% respectively
Outlet pressure	Zero
Absorber plate	No slip condition, stationary wall, heat flux = 850W/m^2, opaque wall
Glass	No slip condition, stationary wall, mixed heat transfer coefficient 9.5 W/m^2 K, free stream temperature and external radiation temperature are 300 K, emissivity = 0.88, and semi-transparent wall

The boundary conditions applied are given in Table 3. The hydraulic diameter is calculated for rectangular channel, and it turns out to be 0.2143 m. The inlet temperature for conventional SAH is 300 K. The local thermal equilibrium model (LTE) is used in the heat transfer from fluid zone to solid porous zone. Hence, the average temperature of glass and absorber plate is taken as inlet temperature for porous solar air heater.

The method used for solution is coupled wall scheme for pressure velocity coupling. The spatial discretization for pressure, momentum, turbulent kinetic energy, and turbulent dissipation rate and energy is second-order upwind scheme. The least square cell-based gradient is used to get more accuracy. The solution controls for pseudo-transient explicit relaxation factors are 0.5, 0.5, 1, 1, 0.75, 1, and 1 for pressure, momentum, density, body forces, turbulent kinetic energy, turbulent dissipation rate, and turbulent viscosity and energy, respectively. The residual for the energy is 10^{-6}. The other residual for continuity, momentum, and turbulent kinetic energy and dissipation are 10^{-4}.

3.2 Governing Equations

For fluid flow in solar air heater, continuity and Reynolds-averaged-Navier–Stokes (RANS) equations are used. In this study, the RNG k-ε turbulence model [5, 14] is used as it improves the performance for rotation and streamline curvature.

$$\text{Continuity equation, } \frac{\partial(\rho u_j)}{\partial x_i} = 0 \tag{1}$$

$$\text{Momentum equation } \frac{\partial}{\partial x_j}(\rho u_i u_j) + \frac{\partial p}{\partial x_i}$$

$$= \frac{\partial}{\partial x_j}\left[\mu\left(\frac{\partial u_i}{\partial x_j} + \frac{\partial u_j}{\partial x_i}\right)\right] + \frac{\partial}{\partial x_j}\left[\mu_t\left(\frac{\partial u_i}{\partial x_j} + \frac{\partial u_j}{\partial x_i}\right)\right] \tag{2}$$

$$\text{Energy equation } \frac{\partial}{\partial x_i}(\rho u_j T) - \frac{\partial}{\partial x_j}\left[(\Gamma + \Gamma_T)\frac{\partial T}{\partial x_J}\right] = 0 \tag{3}$$

where $\Gamma_T = \mu_t/\text{Pr}$ is the turbulent thermal diffusivity, $\Gamma = \mu/\text{Pr}$ is the molecular thermal diffusivity, Pr is the Prandtl number, μ and μ_t are the viscosity (Ns/m^2) and thermal viscosity, respectively, ρ is the density (kg/m^3), P is the pressure (Pascal), u is the velocity (m/s), and T is the temperature (K). To model flow through porous media, it is required to add an additional source term to governing flow equations by using the Forchheimer equation as given below as per [14]

$$\nabla p^* = \frac{\mu}{\alpha}u^* + \beta\rho u^{*2} \tag{4}$$

$$F_i = -\left(\frac{\mu}{\alpha}u_i + C_2\frac{1}{2}\rho|u|u_i\right) \tag{5}$$

where F_i is the source term for the i-th Navier–stokes equation and $C_2 = 2\beta$

For solar air heater with empty channel, hydraulic diameter and Reynolds number are considered.

Local thermal equilibrium model assumes that the solid and fluid phases of the porous medium are in thermal equilibrium, i.e., $Ts = Tf = T$. The net heat transfer between the phases of the porous medium is zero since the heat conduction in both the phases takes place simultaneously.

$$\text{For solid}(1 - \varepsilon)(\rho c)_s\frac{\partial T_s}{\partial t} = (1 - \varepsilon)\nabla \cdot (k_s\nabla T_s) + (1 - \varepsilon)q_s''' \tag{6}$$

$$\text{For fluid } \varepsilon(\rho c_p)_f\frac{\partial T_f}{\partial t} + (\rho c_p)_f U.\nabla T_f = \varepsilon\,\nabla.(k_f\nabla T_f) + \varepsilon\,q_f''' \tag{7}$$

Adding Eqs. (6) and (7)

$$(\rho c)_{eff}\frac{\partial T}{\partial t} + (\rho c)_f U.\nabla\text{T} = \nabla.(k_{eff}\nabla\text{T}) + q_{eff}''' \tag{8}$$

where

$$(\rho c)_{eff} = (1 - \varepsilon)(\rho c)_s + \varepsilon(\rho c_P)_f \tag{9}$$